ENGINEERING EXPERIMENT STATION
DEPARTMENT OF MECHANICAL
AND INDUSTRIAL ENGINEERING
ME-TN-242-2

UNPUBLISHED PRELIMINARY DATA

SOME INFLUENCES OF MACROSCOPIC CONSTRICTIONS ON THE THERMAL CONTACT RESISTANCE

by
A. M. CLAUSING

Research Sponsored by
NATIONAL AERONAUTICS AND SPACE ADMINISTRATION
under Grant NsG-242-62

UNIVERSITY OF ILLINOIS
URBANA, ILLINOIS
APRIL, 1965

ME TECHNICAL REPORT 242-2 April, 1965

SOME INFLUENCES OF MACROSCOPIC CONSTRICTIONS ON THE THERMAL CONTACT RESISTANCE

by

A. M. Clausing

RESEARCH GRANT NO.

NASA NsG-242-62

Department of Mechanical and Industrial Engineering
Engineering Experiment Station
University of Illinois
Urbana, Illinois

Acknowledgment

This research was sponsored by the National Aeronautics and Space Administration under Grant NsG-242-62. The author hereby records his sincere appreciation for this financial support.

The author would also like to express his thanks to Messrs. Rott, McNary, and Cheema, who helped in taking the experimental data and in other phases of this research. The numerical calculations were performed on the IBM-7094 digital computer in the Department of Computer Science at the University of Illinois.

Foreword

The research was carried out under Research Grant No. NsG-242-62, "Theoretical and Experimental Study of Thermal Contact Resistance in a Vacuum Environment."

It was established in the previous technical note (ME-TN-242-1) that macroscopic effects often dominate the thermal contact resistance in a vacuum environment. A restrictive analysis based on a new model was proposed for the prediction of the thermal contact resistance, and extensive results were given which supported the conceptual correctness of the model.

The present technical note gives several extensions of this study. Section 1.0 gives a numerical solution for the constriction resistance which removes the error present in the approximate analytical solution previously employed. In addition, the solution obtained is also valid for thin regions. Previously, the constriction resistance for thin plates could not be predicted even when the contact geometry was defined.

Section 2.0 applies the model in the analysis of contacts between dissimilar metals. It was found that the model is applicable to contacts between dissimilar metals if the influences of thermal strain are small. On the other hand, if thermal strain is of importance, the model is capable of qualitative prediction of the resulting directional effect.

TABLE OF CONTENTS

Nomenclature

a	radius of a contact area
b	radius of constriction region
d	equivalent flatness deviation (see Fig. 1.1)
E	modulus of elasticity
$f(x)$	defined by Equation 1.19
h	interface conductance, $h = \frac{1}{A_a R}$
k	thermal conductivity
L	length of specimen
ΔL	equivalent length of contact resistance
P	load
p	contact pressure
q	heat flux
Q	rate of heat flow
R	resistance
R^*	dimensionless resistance (see Eq. 1.17)
T	temperature
ΔT	a temperature difference
x	constriction ratio, $x = a/b$
z	axial coordinate
α	coefficient of linear expansion
δ	grid spacing, $\delta = \Delta r = \Delta z$
ζ	elastic conformity modulus
ω	relaxation parameter

Subscripts

1	surface or specimen 1
2	surface or specimen 2
a	apparent contact area
c	constriction
L	macroscopic constrictions or contact regions
m	a mean value as defined in text
s	microscopic constrictions or contact areas
t	total

1.0 The Influences of the Region Geometry on the Macroscopic Constriction Resistance

Figure 1.1 represents the model of the contact surface which was employed in the analysis of thermal contact resistance in Reference 1. It was found in this reference that the thermal contact resistance was dominated by the macroscopic constriction resistance. Thus, later analysis has emphasized the study of this resistance.

The determination of the additional temperature drop due to the presence of a constriction consists of two parts: a) Given the load, what is the macroscopic contact area? and b) Given the macroscopic contact area, what is the constriction resistance? Once the constriction resistance is known, the additional temperature drop due to the presence of the interface can be easily calculated. The discussion and analysis which follows pertains to the second problem; i.e., finding the constriction resistance when the macroscopic contact area is known.

For the model proposed in [1]*, the macroscopic contact area was assumed to consist of a single circular contact area of radius a_L whose center coincides with that of the apparent contact area. Thus, the non-contact region is an annulus whose inside and outside radii are a_L and b_L, respectively. Since the geometry, as defined, is symmetrical with respect to the contact plane, the cylindrical region represented by one of the specimens can be considered. It is shown in Figure 1.2 (page 3). Assuming that a perfect contact exists over the region of radius a_L, the following partial differential equation and boundary conditions describe the temperature field:

$$\frac{\partial^2 T}{\partial r^2} + \frac{1}{r}\frac{\partial T}{\partial r} + \frac{\partial^2 T}{\partial z^2} = 0 \qquad (1.1)$$

---

*Numbers in brackets, [..], indicate references listed in Appendix B.

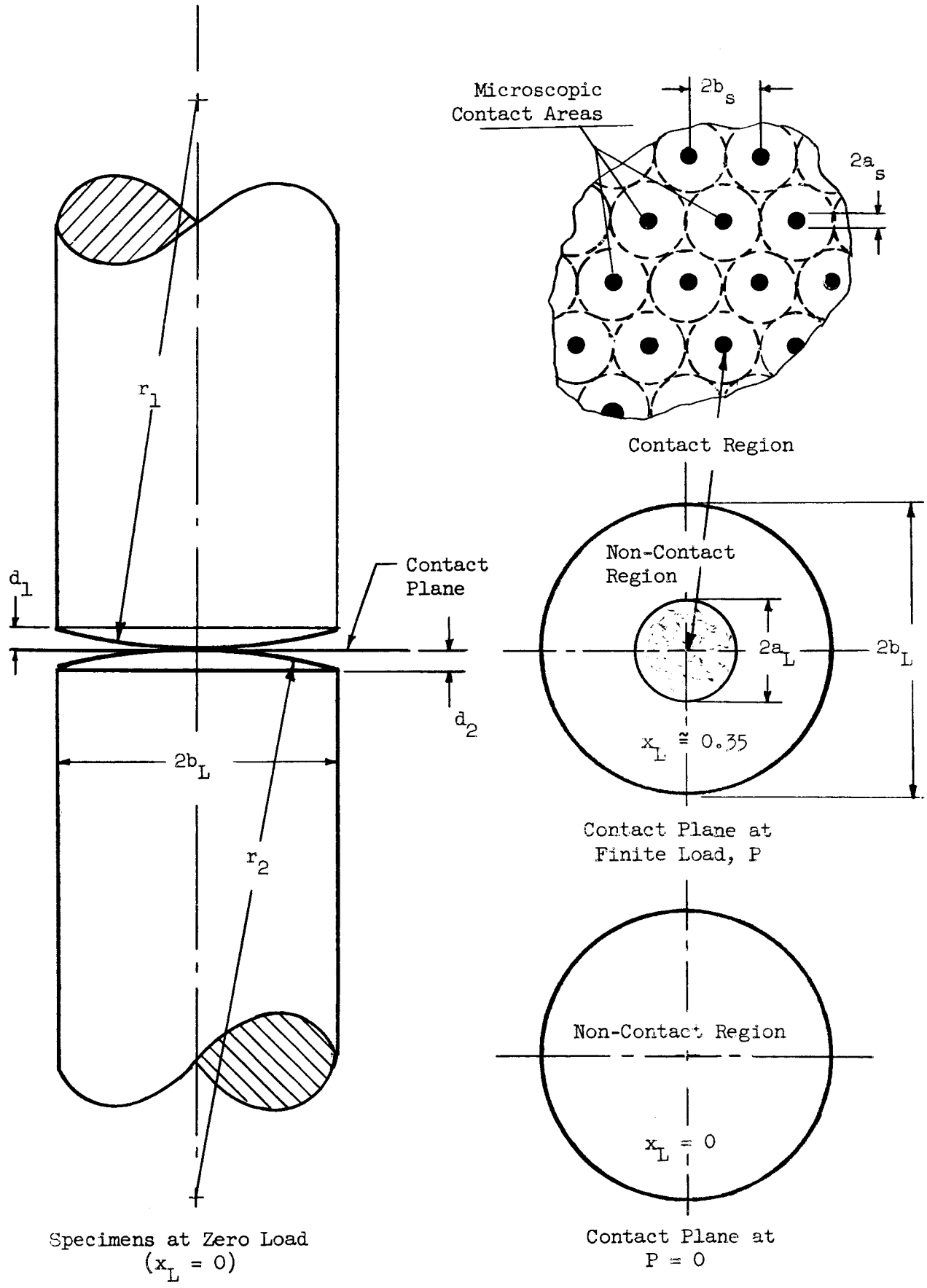

Fig. 1.1 Model of Contact Surface

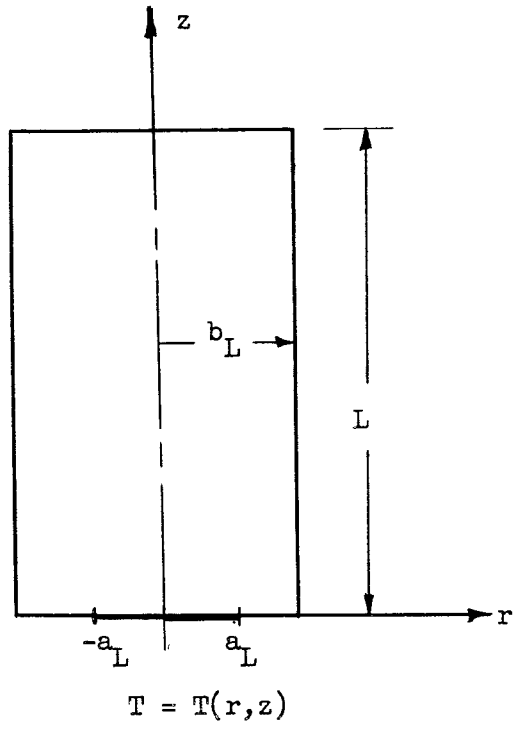

FIGURE 1.2

FINITE CYLINDRICAL REGION

$$T(r,o) = T_o, \qquad 0 \le r \le a_L \tag{1.1a}$$

$$\frac{\partial T}{\partial z}(r,o) = 0, \qquad a_L < r \le b_L \tag{1.1b}$$

$$\frac{\partial T}{\partial r}(b_L,z) = 0, \qquad 0 < z < L \tag{1.1c}$$

$$T(r,L) = T_L, \qquad 0 \le r \le b_L \tag{1.1d}$$

This problem is a very formidable one due to the mixed boundary condition at z = 0. The boundary is isothermal for $0 \le r \le a_L$, whereas there is zero heat flux over the remainder of the boundary, i.e., for $a_L < r \le b_L$. The difficulty due to this mixed boundary condition was circumvented by Roess [8], who found that a flux distribution across the area $0 \le r \le a_L$ which was proportional to $(1 - r^2/a_L^2)^{-1/2}$ resulted in an approximately isothermal area unless the constriction ratio x_L (= a_L/b_L) was near unity. In addition, Roess assumed L/b_L was sufficiently large that the constriction resistance was independent of L/b_L (see Figure 1.2). With these additional assumptions he found the constriction resistance was:

$$R(x_L) = \frac{g(x_L)}{4\, a_L k} \tag{1.2}$$

where

$$g(x_L) = 1 - 1.40925\, x_L + 0.29591\, x_L^3 + 0.05254\, x_L^5 + 0.02105\, x_L^7 + 0.01107\, x_L^9 + \ldots. \tag{1.3}$$

and k is the thermal conductivity. This solution was employed in the analysis given in [1]. The experimental data were then compared with the resulting theoretical prediction.

Further analysis of this was deemed highly desirable since:

(i) Roess' solution failed if $L/b_L < 1$. This region is probably the most important one, especially in the study of thermal contact resistance problems connected with space vehicles where thin plates are often employed. Under such circumstances, small values of L/b_L would be present and the theoretical prediction of [1] would no longer be applicable.

(ii) The theoretical solution of [1] which employed Roess' solution predicted smaller values of the constriction resistance than the experimental values if x_L was near unity. Part of this discrepancy could be due to the failure of Roess' solution to apply, since his assumed flux distribution is in error if x_L is near unity.

1.1 Solution Procedure

Analytically, little success has been achieved in solving problems with mixed boundary conditions such as the one given. This fact combined with the limited success which Roess obtained indicated that a numerical approach would probably be most rewarding. The only anticipated difficulty which the mixed boundary condition should cause in a numerical solution is relatively large spatial truncation errors in the region near the point of intersection of the isothermal boundary and the zero flux boundary, $z = 0$, $r = a_L$. One can see that the derivatives will be large near this point; thus, large spatial truncation errors will result. If a sufficiently fine network were employed in order to reduce these errors to acceptable proportions, it was initially thought that the computation time might be excessive. However, it was possible to circumvent

this problem.

1.1.1 The Difference Equations Employed

If one takes advantage of the symmetry of the region, a possible nodal network is that given in Figure 1.3. In the finite difference representation of (1.1), Δr was chosen equal to Δz. The subscripts "i" and "j" refer to the z and r directions respectively. Each increases with an increase in the corresponding independent variable.

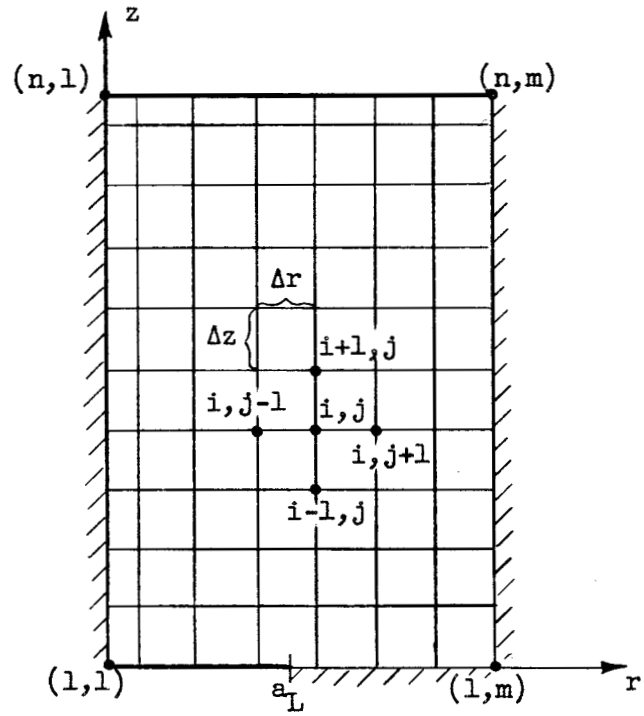

FIGURE 1.3

A finite difference representation of Equation (1.1) is:

$$T_{i-1,j} + T_{i+1,j} + \left(1 + \frac{\Delta r}{2r_j}\right) T_{i,j+1} + \left(1 - \frac{\Delta r}{2r_j}\right) T_{i,j-1} - 4\, T_{i,j} = 0 \qquad (1.4)$$

where r_j is the radius corresponding to the j-th column and $\Delta r = \Delta z = r_{j+1} - r_j$. The thermal conductivity has been assumed to be constant. However, by an appropriate change in the dependent variable, the case of a linear variation of the conductivity with temperature could have been treated with negligible additional computation time and no further complication. Equation (1.4) is valid for all nodal points except those lying on the boundaries of the region. "n" stands for the number of rows and "m" stands for the number of columns. Since Δr was chosen equal to Δz, the ratio of the length L to the radius b_L is given by:

$$\frac{L}{b_L} = \frac{n - 1}{m - 1} \quad .$$

For the nodal points on the r = 0 boundary, the simple equation

$$T_{i,1} = T_{i,2} \tag{1.5}$$

was employed. The error introduced by this approximation was always negligible. If this error is of importance, it can be easily detected by the failure of the solution to satisfy a heat balance. At the right insulated boundary the difference equation becomes:

$$T_{i-1,m} + T_{i+1,m} + 2(1 - \frac{\Delta r}{2r_m}) T_{i,m-1} - (4 - \frac{\Delta r}{r_m}) T_{i,m} = 0 \tag{1.6}$$

Likewise, a difference equation for nodal points on the lower insulated boundary is:

$$2T_{2,j} + (1 + \frac{\Delta r}{2r_j}) T_{1,j+1} + (1 - \frac{\Delta r}{2r_j}) T_{1,j-1} - 4T_{2,j} = 0 \tag{1.7}$$

Finally, a difference equation for the nodal point at the insulated right hand lower corner is:

$$2T_{2,m} + 2(1 - \frac{\Delta r}{2r_m}) T_{1,m-1} - (4 - \frac{\Delta r}{r_m}) T_{1,m} = 0 \tag{1.8}$$

Thus, all the necessary difference equations are known since the remainder of the boundary is at some known temperature. Note that the point $r = a_L$, $z = 0$ has been conveniently placed midway between two nodal points.

The total number of unknowns is $[(n-1)\, m - m_a]$, where m_a is the number of nodal points on the lower isothermal boundary. The resulting simultaneous algebraic equations are of the form:

$$\begin{aligned}
a_{11} x_1 + a_{12} x_2 + \cdots + a_{1n} x_n &= c_1 \\
a_{21} x_1 + a_{22} x_2 + \cdots + a_{2n} x_n &= c_2 \\
\cdots & \\
a_{n1} x_1 + a_{n2} x_2 + \cdots + a_{nn} x_n &= c_n
\end{aligned} \tag{1.9}$$

Equations (1.9) can be rewritten as:

$$\begin{aligned} x_1 &= \frac{1}{a_{11}} (c_1 - a_{12} x_2 - a_{13} x_3 - \cdots - a_{1n} x_n) \\ x_2 &= \frac{1}{a_{22}} (c_2 - a_{21} x_1 - a_{23} x_3 - \cdots - a_{2n} x_n) \\ &\cdots \\ x_n &= \frac{1}{a_{nn}} (c_n - a_{n1} x_1 - a_{n2} x_2 - \cdots - a_{n,n-1} x_{n-1}) \end{aligned} \tag{1.10}$$

In this form the equations are amenable to an iterative process. If the x's are calculated in their natural order, the procedure is called the Gauss Seidel iteration. When applied to elliptic difference equations, the procedure is also known as the method of successive displacements or the Liebmann Method. For the set of difference equations which we obtained, convergence of the Gauss Seidel iteration is guaranteed since a sufficient condition for convergence is [2]:

$$|a_{ii}| \geq |a_{i,1}| + \cdots + |a_{i,i-1}| + |a_{i,i+1}| + \cdots + |a_{in}|$$

for all i, and for at least one i:

$$|a_{ii}| > |a_{i,1}| + \cdots + |a_{i,i-1}| + |a_{i,i+1}| + \cdots + |a_{in}|$$

These conditions are satisfied by the difference equations given.

1.1.2 Methods Used to Decrease the Computation Time

If Equations (1.10) are rewritten as:

$$\begin{aligned} x_1' &= x_1(1 - \omega) + \frac{\omega}{a_{11}} (c_1 - a_{12} x_2 - a_{13} x_3 - \cdots - a_{1n} x_n) \\ x_2' &= x_2(1 - \omega) + \frac{\omega}{a_{22}} (c_2 - a_{21} x_1 - a_{23} x_3 - \cdots - a_{2n} x_n) \\ &\cdots \\ x_n' &= x_n(1 - \omega) + \frac{\omega}{a_{nn}} (c_n - a_{n1} x_1 - a_{n2} x_2 - \cdots - a_{n,n-1} x_{n-1}) \end{aligned} \tag{1.11}$$

where $0 < \omega < 2$, we have the extrapolated Liebmann method. "ω" is called the

relaxation parameter. If $\omega = 1$, Equations (1.11) reduce to (1.10) and the iterative scheme becomes the Gauss Seidel iteration. The employment of $\omega > 1$ is similar to "overrelaxation" and $\omega < 1$, "underrelaxation" in solving problems by the relaxation technique. If $\omega = 1$, the residue at a nodal point is reduced to zero when a new value of the dependent variable is calculated at this point. If ω were 2, the magnitude of the residue would not be affected; only its sign would change.

The extrapolated Liebmann method as described was employed in obtaining the solution to the resulting set of difference equations. This iterative scheme was considerably faster than the ordinary Gauss Seidel iteration. In addition, several other techniques were employed in order to decrease the computation time and spatial truncation error. These techniques follow.

It is well known that the number of iterations required to converge to the solution of a set of simultaneous equations (assuming the scheme is convergent) is highly dependent on the initial guess. The time required for one iteration also increases greatly as the number of equations is increased. For these reasons, a solution was first obtained with a relatively crude subdivision. Δr and Δz were then decreased by a factor of three which resulted in approximately nine times as many simultaneous equations as contained in the initial network. The temperatures at the new additional nodal points were determined by linear interpolation. Thus, although the number of simultaneous equations solved was often greater than 2700, the total number of iterations required was usually less than 300. An extremely useful by-product of this procedure was that the spatial truncation error could be rationally estimated since the unknowns were evaluated for several different nodal spacings. The nodal spacing was changed by factors of three instead of two as a consequence of the point $r = a_L$, $z = 0$ (see Figure 1.3).

It is known that the derivatives are large in the region of $z = 0$, $r = a_L$.

If a uniform network is employed, the number of equations required in order to reduce the spatial truncation error in this region to a negligible amount is very large. Since such a large number of equations would require considerable computation time, a nonuniform network was employed. A finer nodal spacing was employed only for a small annular region centrally located with respect to the point $z = 0$, $r = a_L$. The values of Δr and Δz for the fine network were 1/3 of the values employed in the coarse network.

One of the major reasons for this effort was to determine the dependence of the constriction resistance, R_c, on the length of the region L. It is known that as L/b_L becomes large, R_c is independent of L/b_L and $\partial T/\partial z$ becomes a constant. This latter fact was employed in order to speed the computation process. A solution was obtained for the smallest value of L desired, which will be called L_1. The length of the region was then increased to L_2 and the previous results were used as an initial guess for $z \leq L_1$. For $L_1 < z \leq L_2$ a value of $\partial T/\partial z$, which was based on the total rate of heat flow, Q, was determined and the initial guess for the region was then obtained by assuming that this gradient was a constant. The new boundary temperature at $z = L_2$ is given by:

$$T_{L(new)} = T_{L(old)} - \frac{Q(L_2 - L_1)}{k \pi b_L^2} \tag{1.12}$$

The length L was incremented until Q became approximately constant; i.e., until R_c became independent of L. The constriction resistance could be determined as a function of L by this procedure with a considerable savings in computer time. When the initial approximation is poor, the number of equations is small. As L (and hence the number of equations) approaches infinity, the error in the initial approximation approaches zero. It was found that R_c could be determined for a series of values of L by employing this procedure in approximately the same computation time as that required if R_c were calculated for only the largest value of L in the series.

1.2 Results of Numerical Computations

Since it is difficult for the reader to assess the accuracy of the results of a numerical calculation if a basis for the reported accuracy is not given, a discussion of the accuracy of the numerical results will first be given.

Two important sources of error can arise: spatial truncation error and error caused by obtaining the solution to a set of simultaneous equations by an iterative scheme, an infinite mathematical process, in a finite number of operations. Round-off error did not cause any problems for the iterative procedure employed. As a_L approaches zero the difference equations become ill-conditioned as can be seen from physical arguments. However, the degree of ill-conditionness was never sufficient for the range of x_L employed to cause computational difficulty. (The computational time did increase as x_L became small.)

The error caused by truncating the iterative procedure after a finite number of iterations was assessed from an energy balance. Neglecting the effect of the approximation employed at the centerline of the region, the heat flowing into the region will equal the heat flowing out of the region, in general, only if the iterative procedure has converged to the solution of the finite difference equations. An energy balance was therefore employed as a convergence check. This check is excellent since the constriction resistance is calculated directly from the heat flow rate. The error in the total resistance is the same as the error in Q. The total resistance is given by:

$$R_t = \left| \frac{T_L - T_o}{Q} \right| \tag{1.13}$$

and the constriction resistance is given by:

$$R_c = R_t - \frac{L}{k \pi b_L^2} \tag{1.14}$$

The rate of heat flow Q was determined from the average of $(Q_{z=o} + Q_{z=L})/2$.

When the heat flowing through the boundary at z = 0 was within 1%, 0.5%, and 0.25% of the heat flowing out of the boundary at z = L, the unknowns were printed. These results showed that the average of these two heat flow rates was always considerably more accurate than the percentage difference between them. Thus, it is estimated that the error in R_t caused by truncating the iterative process was always less than 0.05%. (In some cases, $Q_{z=o}$ was within 10^{-5} per cent of the heat flow rate, $Q_{z=L}$, before the convergence test was made.) It follows from (1.14) that the error in R_c is largest when R_c is small compared with R_t. This maximum error which occurred for $x_L = 0.833$ was only 1%. This error is 0.003% for $x_L = 0.3$.

It can easily be shown that the spatial truncation error is of the order of the square of the nodal spacing which is $\Delta r = \Delta z = \delta$. If the fourth derivatives are relatively constant, one can assume that the spatial truncation error is proportional to δ^2. Thus, the true constriction resistance becomes:

$$R_c = R_{c1}' + c\,\delta_1^2 \tag{1.15}$$

where R_{c1}' is the numerical value obtained with a nodal spacing of δ_1. Since two different interval sizes were used in the calculation scheme employed, it is also known that:

$$R_c = R_{c2}' + c\,\delta_2^2$$

Thus, the true value is given by:

$$R_c = R_{c1}' - \frac{R_{c1}' - R_{c2}'}{1 - (\delta_1/\delta_2)^2} \tag{1.16}$$

Calculations using a multiple of nodal spacings indicated that (1.16) not only provided a good indication of the magnitude of the spatial truncation error but also a means of removing part of this error. Thus, small corrections were

applied to the numerical results using Equation (1.16). This correction never exceeded 0.6%. The results indicated that the spatial truncation error is probably less than 1% although for some of the limiting cases this error may be slightly larger.

A dimensionless constriction resistance R_c^* will be defined as:

$$R_c^* = \frac{k R_c \pi b_L^2}{b_L} = \frac{k}{h b_L} = \frac{\Delta L}{b_L} \qquad (1.17)$$

where ΔL may be interpreted as the additional length of the region required to produce the same resistance as the constriction. This is the same dimensionless resistance as was employed in the dimensionless plots of [1]. The subscript "c" is employed only to differentiate the constriction resistance from the total resistance. Since it is the only resistance being considered in many discussions, the subscript is often dropped.

The results obtained from the numerical solution are given in Table 1.1. These values are the dimensionless constriction resistance as defined by (1.17) and are the constriction resistance of <u>one</u> region only. For two cylindrical regions of the same length and radius in contact over a circular, concentric area of radius a_L, the total constriction resistance or the so-called contact resistance is <u>twice</u> the value given in Table 1.1.

Table 1.2 shows the variation of the ratio $R_c^*(L/b_L)/R_c^*(L/b_L=\infty)$ with x_L and L/b_L. The variation of the constriction resistance with L/b_L is clearly shown in these tables. These data show that the macroscopic constriction resistance is large even for relatively thin plates. For example, consider a disk 0.2" thick and 2" in diameter with a constriction ratio of 0.5. Its constriction resistance is still 71% of the value for $L=\infty$. If its thickness were 0.067", this value would be reduced to 32%. Thus, it is seen that <u>macroscopic effects also will be dominant for thin plates</u>, provided these effects are dominant for thick regions. The dominance for thick regions was shown in [1].

$R_c^* = \Delta L/b_L$

L/b_L \ x_L	.167	.233	.300	.367	.433	.500	.567	.633	.700	.767	.833
0.0	0	0	0	0	0	0	0	0	0	0	0
.0667	1.689	0.906	.552	.360	.247	.173	.122	.0856	.0589	.0389	.0231
.1333	2.542	1.446	.911	.6080	.4216	.2970	.210	.1460	.0990	.0630	.0352
.200	3.000	1.772	1.145	.7760	.5425	.3830	.270	.1861	.1240	.0765	.0407
.267	3.257	1.972	1.299	.8878	.6237	.4410	.3090	.2115	.1387	.0836	.0434
.4	3.494	2.169	1.452	1.006	.7105	.5014	.3495	.2360	.1522	.0897	.0452
.6	3.597	2.258	1.526	1.063	.7523	.5306	.3680	.2470	.1575	.0919	.0459
.8	3.618	2.277	1.542	1.077	.7615	.5368	.3720	.2493	.1584	.0923	.0459
1.0	---	2.281	1.544	1.080	.7636	.5380	.3728	.2498	.1585	.0924	.0460
1.2	---	---	---	---	.764	---	.3729	---	---	---	---
∞	3.625	2.283	1.545	1.080	.764	.539	.373	.250	.159	.0924	.0460

Table 1.1 The Dimensionless Constriction Resistance R_c^* as a Function of x_L and L/b_L

$R_c(L/b_L)/R_c(L/b_L = \infty)$

L/b_L \ x_L	.167	.233	.300	.367	.433	.500	.567	.633	.700	.767	.833
0	0	0	0	0	0	0	0	0	0	0	0
.0667	.466	.397	.357	.333	.324	.321	.327	.342	.370	.421	.502
.1333	.703	.632	.590	.563	.553	.552	.564	.584	.623	.682	.765
.200	.828	.777	.741	.719	.711	.711	.724	.745	.780	.828	.885
.267	.889	.864	.841	.812	.816	.819	.829	.846	.872	.905	.944
.4	.965	.950	.940	.931	.931	.932	.936	.945	.959	.971	.984
.6	.993	.989	.988	.985	.986	.986	.986	.989	.991	.995	.998
.8	.998	.995	.999	.996	.998	.998	.999	.997	.998	.999	.998

Table 1.2 The Ratio $R_c(L/b_L)/R_c(L/b_L = \infty)$ as a Function of x_L and L/b_L

It must be remembered that the boundary conditions for an actual contact between thin regions could be different than those given by (1.1a) to (1.1d). These results could not be directly applied for such cases but could be employed in a qualitative study. The definition of resistance as normally employed would probably no longer be applicable for other types of boundary conditions. Thus, a new, meaningful description of the effects of imperfect thermal contact at interfaces would have to be developed.

Figure 1.4 gives a comparison between the present results and Roess' solution. This comparison clearly shows the error in Roess' approximate solution which was caused by the failure of his assumed flux distribution to adequately approximate the isothermal boundary condition for large values of x_L. If x_L is small, the agreement between the two solutions is excellent. This was expected since Roess' solution is known to agree with the exact solution which is available for the limiting case of $x_L = 0$.

The data of Table 1.1 for the case of $L/b_L > 0.8$ was fitted with a fifth degree least squares polynomial. The resulting equation is:

$$R_c^* = \frac{\Delta L}{b_L} = 10^{f(x_L)}, \qquad \left\{ \begin{matrix} L/b_L > 0.8 \\ .16 < x_L < .84 \end{matrix} \right\} \tag{1.18}$$

where

$$f(x_L) = [1.3983865 - 7.4469788\, x_L + 19.930288\, x_L^2 - 38.589651\, x_L^3 + 38.655295\, x_L^4 - 16.624690\, x_L^5] \tag{1.19}$$

The disagreement between the numerical values and Equation (1.18) was always less than one per cent. The dimensionless contact resistance for two similar regions in contact is:

$$R^* = 2(10^{f(x_L)}), \qquad \left\{ \begin{matrix} L/b_L < .8 \\ .16 < x_L < .84 \end{matrix} \right\} \tag{1.20}$$

Extensions of the numerical procedure given in this section to obtain

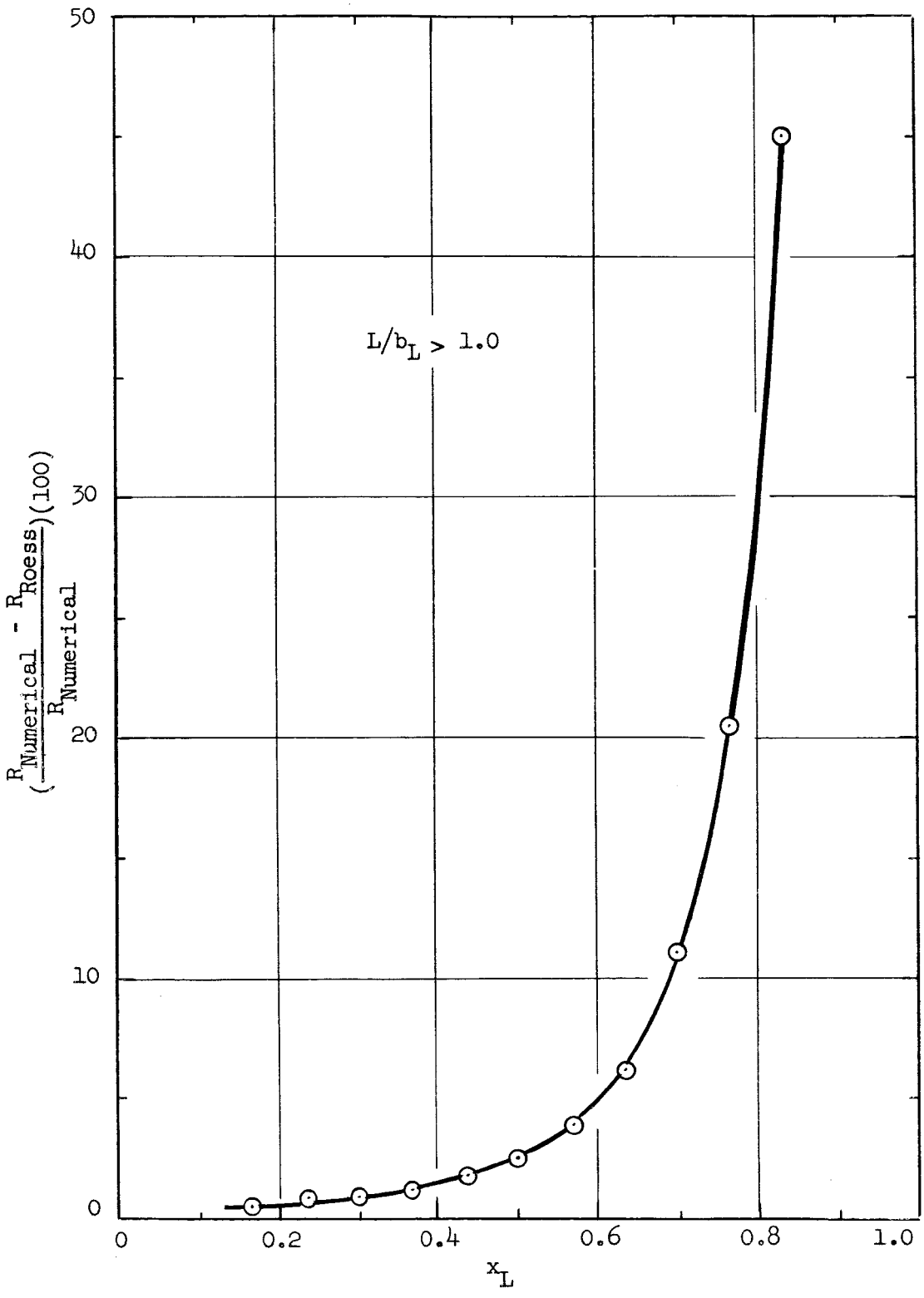

Fig. 1.4 Comparison between Roess' Approximate Solution and the Numerical Solution

solutions to variations of the problem described by Equations (1.1) can easily be made and are being considered. Extensions to the study of the effects of thermal constrictions in transient heat conduction can also be easily made. One such problem which is designed to demonstrate possible consequences of imperfect thermal contacts in transient heat conduction is under consideration.

2.0 Heat Transfer at the Interface of Dissimilar Metals--The Influences of Thermal Strain

The dependence of the thermal contact resistance on the direction of heat flow at an interface between dissimilar metals was first reported by Barzelay, et al. [3]. They found that in some instances the interface conductance for heat flow from aluminum to steel was over five times higher than when the heat flowed in the other direction. Motivated by Barzelay's results, Rogers [4] performed a more detailed experimental study of dissimilar metallic interfaces. His results showed that the interface conductance for an interface in air was approximately 20 per cent higher when heat flowed from aluminum to steel than when it flowed in the other direction. The numerical difference between the values of interface conductance for an interface in vacuum remained approximately the same, but the percentage difference rose to 100%. Rogers found little or no directional effect for chromel-alumel and copper-steel interfaces. He suggested that the effect could be associated with the mechanism of conduction at the "points" of metallic contact. Williams [5] attributed this phenomenon to surface contamination, and Moon and Keeler [6] applied the theory of heat conduction in the solid state to explain this asymmetric behavior. Powell, et al. [7], did not find any directional effect for an aluminum-steel interface or for several other interfaces formed by dissimilar metals which they recently tested. Their measurements were made with a thermal comparator.

It is thus seen that the directional effect is a confusing phenomenon. Barzelay attributed it to warping, whereas Rogers claimed that his results made Barzelay's explanation unacceptable. Others are studying the physics of heat conduction across the "actual" contact areas. At the same time, some data has shown no directional effect. It is not possible to explain or account for the presence of a directional effect with the microscopic models presented in the literature (see [1] for a discussion of these models). Let us now consider this

problem employing the macroscopic model given in [1].

The formation of the microscopic contact areas is usually attributed to plastic deformation between contacting asperities. This means that the thermal stresses caused by microscopic constrictions* are probably small in comparison to the mechanical stresses which were required to cause this plastic deformation; consequently, the influence of these temperature gradients on the microscopic contact areas is small. On the other hand, the mechanical stresses and accompanying strains which cause the formation of the macroscopic contact areas are usually small, since thermal contact resistance is a major problem only if the loads between the contacting surfaces are small, and since the flatness deviations of realistic surfaces are not large. It would thus appear that in some instances thermal strain would influence the size of the macroscopic contact area and consequently the macroscopic constriction resistance.

It can be seen from the results presented in [1] that relative strains of only a few microinches in a direction perpendicular to the plane of the interface could appreciably influence the macroscopic contact area. The reader can easily verify, by considering the simple problem of the linear expansion of a rod, that thermal strains of this magnitude could have been present in many of the specimens employed in obtaining the data reported in the literature. It can also be easily shown that strains parallel to the plane of the interface cause a negligible change in the macroscopic constriction.

If it is assumed that one end of the two contacting members is unrestrained, i.e., that the load exerted between the contacting members is constant and not affected by the longitudinal expansion or contraction of the contacting members,

---

* This discussion excludes the thermal strains due to a change in the temperature level of the regions. These strains would cause a relative motion between the contacting surfaces which would cause a change in the microscopic contact areas. However, these changes would occur in all joints, and although they add considerable complication to a microscopic deformation model, they cannot account for a directional effect.

thermal strain affects the macroscopic constriction resistance only when temperature gradients parallel to the plane of contact are present. Such gradients will result if: (i) macroscopic constrictions to the heat flow across the interface are present, or (ii) the thermal boundary conditions caused by the environment permit heat flow parallel to the plane of contact. These two sources of strain will be considered separately.

2.1 Thermal Strain Resulting from Macroscopic Constrictions

Consider the physical model of the contacting members employed in [1]; i.e., two cylindrical isotropic regions of length L and identical radius b_L. The flatness deviation of the contacting surfaces is simulated by spherical caps of radii r_1 and r_2. It will be further assumed momentarily that the coefficient of linear expansion of the lower member is zero.

It can be seen from Figure 2.1 that if heat is flowing from the upper member to the lower member, the portion of the upper member near the macroscopic contact area is cold relative to the rest of the member. Thus, this region contracts, which causes the formation of a larger macroscopic contact area than that which is predicted if only the mechanical stresses are considered (see Fig. 2.1). If the direction of heat flow is reversed, the portion of the upper member near the macroscopic contact is hot relative to the remainder of the member. In this case, the thermal strain causes a smaller macroscopic contact area than that which is predicted from the mechanical stresses. Thus, it is seen that if the heat is flowing from the upper to the lower member, the thermal strain causes a decrease in the macroscopic constriction resistance, whereas if it is flowing in the other direction, the thermal strain causes an increase in the macroscopic constriction resistance. The thermal contact resistance thus becomes a function of the direction of heat flow.

The geometry of the contacting members will obviously influence the size of

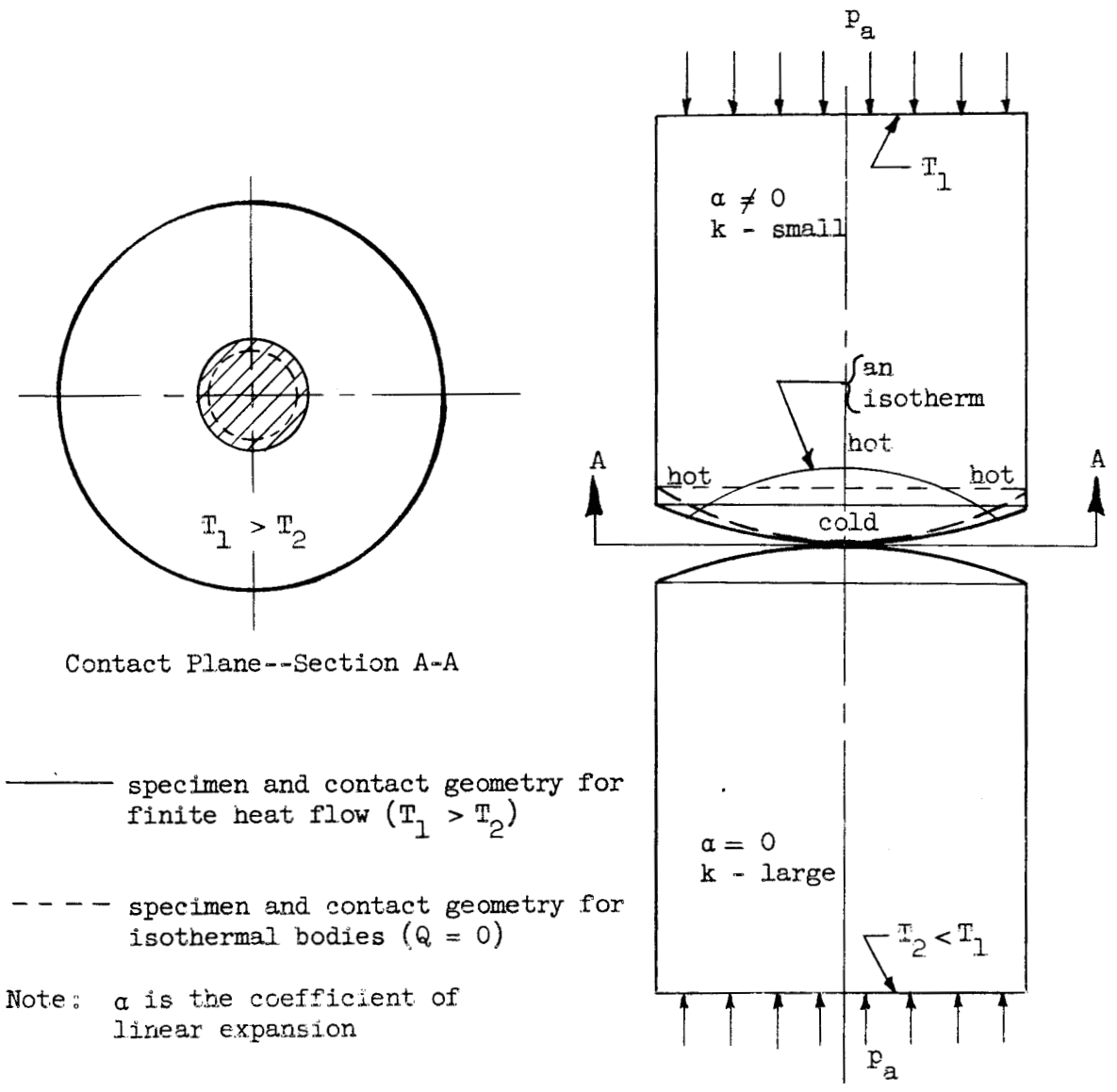

Figure 2.1 Effect of Thermal Strain Resulting from a Macroscopic Constriction

the macroscopic contact area and the manner in which the size of this area varies with the mechanical load. However, the trend of the directional effect is seen to be independent of the geometry of the contacting surfaces. For example, consider the case when the heat is flowing from the upper specimen to the lower specimen. The regions near the macroscopic contact area in the upper specimen will be cold relative to the surrounding region of the specimen. The thermal strain for this case will cause the macroscopic contact area to grow whether the

upper contacting surface is concave or convex. (The lower surface could also be either concave or convex.)

The amount of thermal strain which occurs is a function of the coefficient of linear expansion α, the modulus of elasticity E, Poisson's ratio ν, and the magnitude of the temperature gradients. Thus the influence of thermal strain is dependent on the heat flux and the thermal conductivity of the material. If the heat flux is small and the thermal conductivity is large, the influences of thermal strain vanish.

Now, consider a contact formed between two identical materials where both the upper and lower regions have the same coefficient of linear expansion. If the material properties are independent of temperature, the thermal strains perpendicular to the interface which occur in the regions as a consequence of macroscopic constrictions are complementary; thus the macroscopic contact area is approximately the same as that present in the absence of thermal strain. Since the variation of the material properties with temperature is not large, the neglect of the effect of thermal strain due to macroscopic constrictions should not cause much discrepancy between the theoretical predictions of [1] and the experimental results for contacts between identical materials. Dependency of material properties on temperature will not cause a directional effect in contacts between identical materials as long as the specimen's geometries and the imposed boundary conditions are identical.

When dissimilar metals are in contact, a directional effect is frequently detectable. For a combination such as stainless steel-aluminum, the directional effect is often pronounced due mainly to the large difference in the magnitude of the thermal conductivities. (The thermal conductivity of the aluminum specimens tested was approximately an order of magnitude greater than that of the stainless steel specimens.) At present a theoretical prediction of the influence of each parameter is not possible. A discussion of the role played by each

variable will be delayed until the problem is understood more completely.

2.2 Thermal Strain Due to the Thermal Environment

The importance of small temperature gradients parallel to the plane of the interface has not been realized probably because the importance of slight macroscopic nonconformities of the mating surfaces was previously not realized. However, gradients as small as $1^{\circ}F$ in a direction parallel to the plane of the interface may be of importance. These gradients could arise, for example, from small amounts of radiant heat exchange with the environment or from thermal shunting. (Thermal shunting would occur if an alignment device or an insulating material were in contact with the specimens.) Gradients in a direction parallel to the plane of the interface would be most likely to occur in poor conductors; e.g., stainless steel, since a small heat flux causes a much larger gradient in a poor conductor. Figure 2.2 gives an exaggerated representation of the effect of a small radial gradient on a previously flat surface for the cylindrical geometry employed in [1]. It is seen that in this case the thermal strain may be beneficial or detrimental depending on the original geometry of the contacting

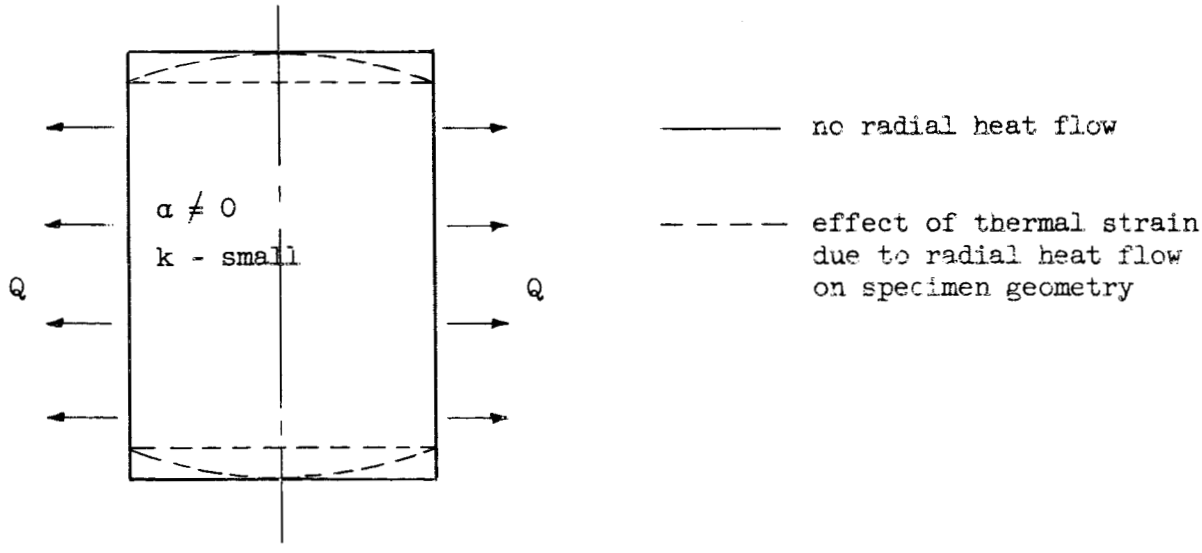

Figure 2.2 Effect of Thermal Strain Due to Thermal Environment

surfaces and on the sign of the radial heat flux. For the geometry employed in [1], the effect was always detrimental since the specimens were losing heat by radiation to the chamber walls in all cases.

This source of thermal strain could also give rise to a directional effect in contacts between dissimilar metals. For example, for a stainless steel-aluminum interface, the heat flow in the stainless specimen would cause the largest gradients; thus geometry changes due to thermal strain in this specimen would have the greatest influence on the macroscopic contact area. Since the temperature level of the stainless steel specimen and therefore the amount of heat it exchanges with its environment would normally vary considerably with the direction of heat flow, a directional effect would result. The influence of these gradients is presently being studied in greater detail.

2.3 Experimental Results*

Figure 2.3 gives a comparison of the experimental results of a stainless steel-aluminum interface which was studied. This interface had a total equivalent flatness deviation of 180 μ in., and the specimens had surface roughnesses of approximately 4 μ in. The dimensionless coordinates suggested in [1] are being employed. E_m and k_m are now the harmonic means based on the values for aluminum and stainless steel. The theory curve which is given in Figure 2.3 does not include the effects of thermal strain. Thus, when the heat flowed from the stainless steel to the aluminum, the resistance was lower than the predicted values due to the enlargement of the macroscopic contact area by thermal strain as discussed in Section 2.1. When the heat flowed from the aluminum to the stainless steel, the thermal contact resistance was greater than the theoretical predictions. These results indicate that the thermal strain due to the macroscopic

* A description of the test surfaces and a tabulation of the experimental results is given in Appendix A.

constriction was dominant. This was expected since the specimen surfaces were highly polished and the heat loss by radiation was small.

The data given in Figure 2.3 were taken with a constant temperature drop across the test column; thus, when the resistance of the interface changed, the heat flux was changed. Of course, the contact resistance is highly dependent on the heat flux for this combination of dissimilar metals and it must be considered in using these data.

It is seen that a single conductance or resistance versus pressure curve is no longer sufficient to describe a given interface between dissimilar metals even in the absence of hysteresis-like variations. If the heat flow rate is employed as a parameter, a family of curves would result. If the thermal strain is due only to the macroscopic constriction and if microscopic effects are unimportant, the theoretical curve given in Figure 2.3 would represent the limiting case of zero heat flux.

Figures 2.4, 2.5, and 2.6 show the variation of the contact resistance with heat flux for this stainless steel-aluminum interface for several different apparent contact pressures. During a given series of tests, the contact pressure was held constant while the heat flow rate was varied from some maximum value to a value near zero. The direction of heat flow was then reversed and the heat flow rate was again increased. The rate of heat flow was changed by changing the source temperature.

It is seen in these figures that as the heat flux approaches zero, the directional effect vanishes. This was to be expected since the thermal strain resulting from the macroscopic constriction approaches zero as the heat flow rate approaches zero, and also the small radial heat loss from the specimen surfaces was virtually eliminated. The heat loss from the specimen surfaces was due to thermal radiation. The sink temperature was fixed at approximately $50^{\circ}F$; the chamber temperature was approximately $75^{\circ}F$; and the source temperature

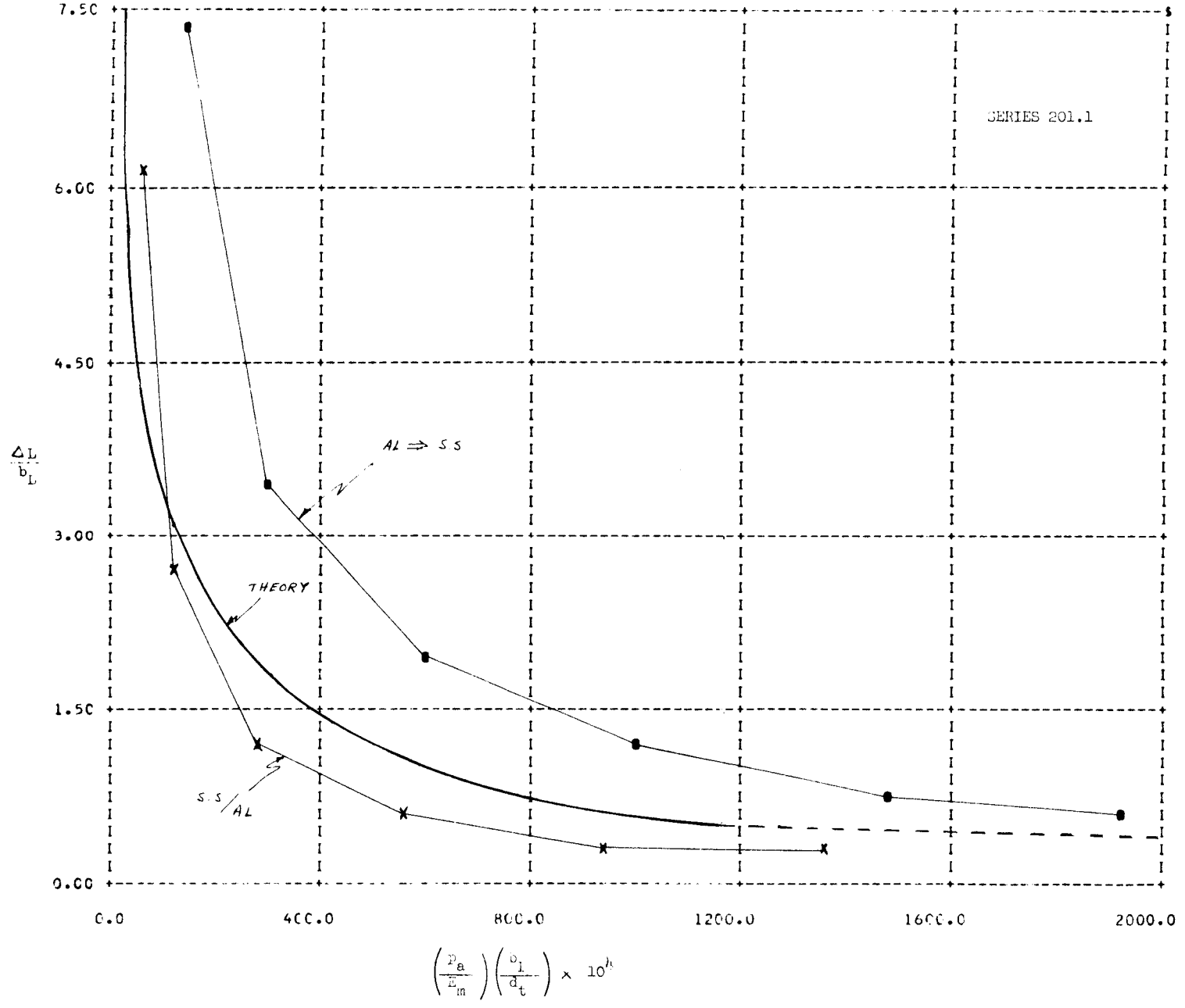

FIGURE 2.3. COMPARISON BETWEEN EXPERIMENTAL RESULTS FOR STAINLESS STEEL-ALUMINUM INTERFACE AND THEORETICAL PREDICTIONS WHICH NEGLECT THERMAL STRAIN EFFECTS

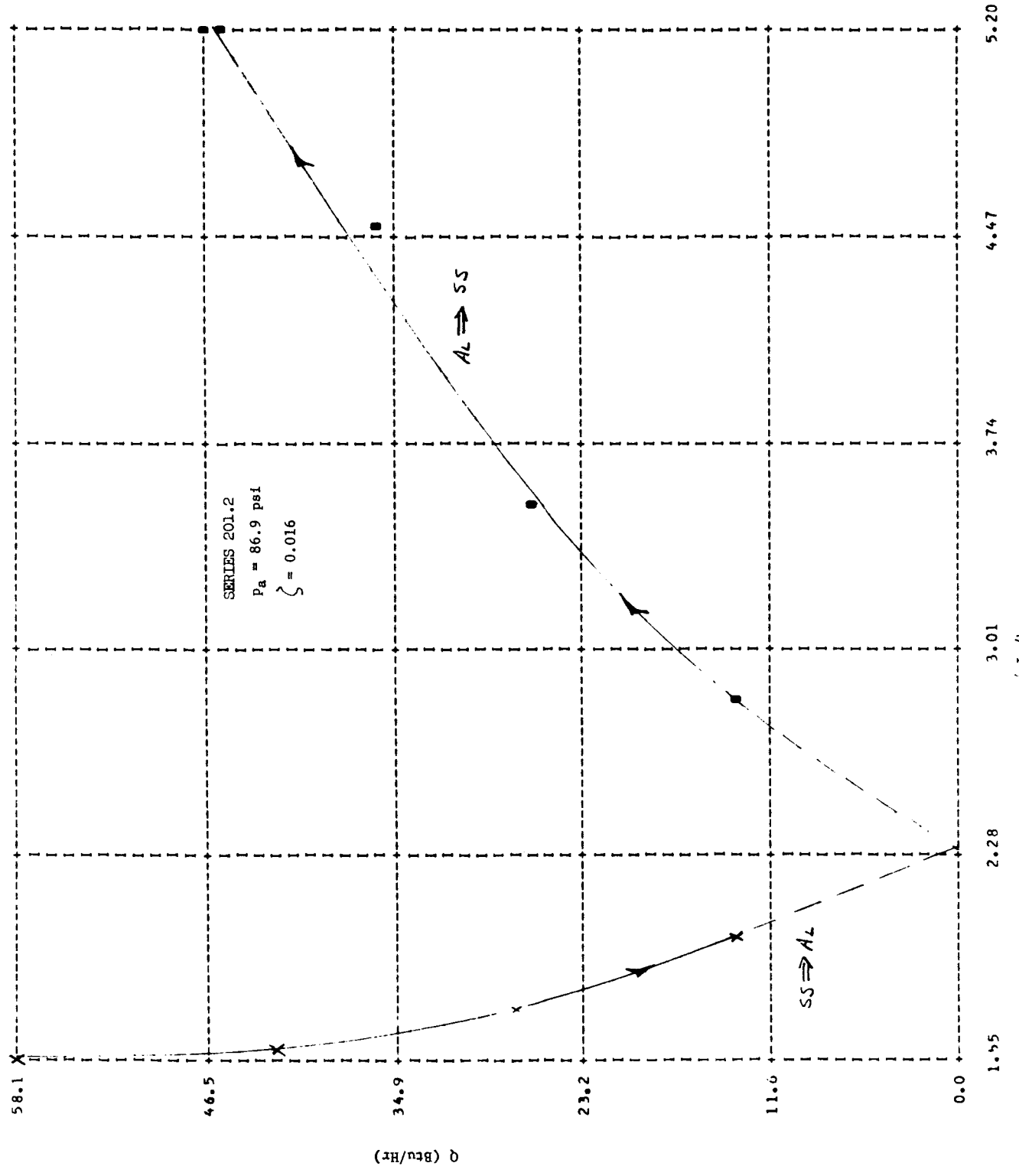

FIGURE 2.4. THE INFLUENCE OF THE RATE OF HEAT FLOW ON THE CONTACT RESISTANCE: STAINLESS STEEL-ALUMINUM INTERFACE

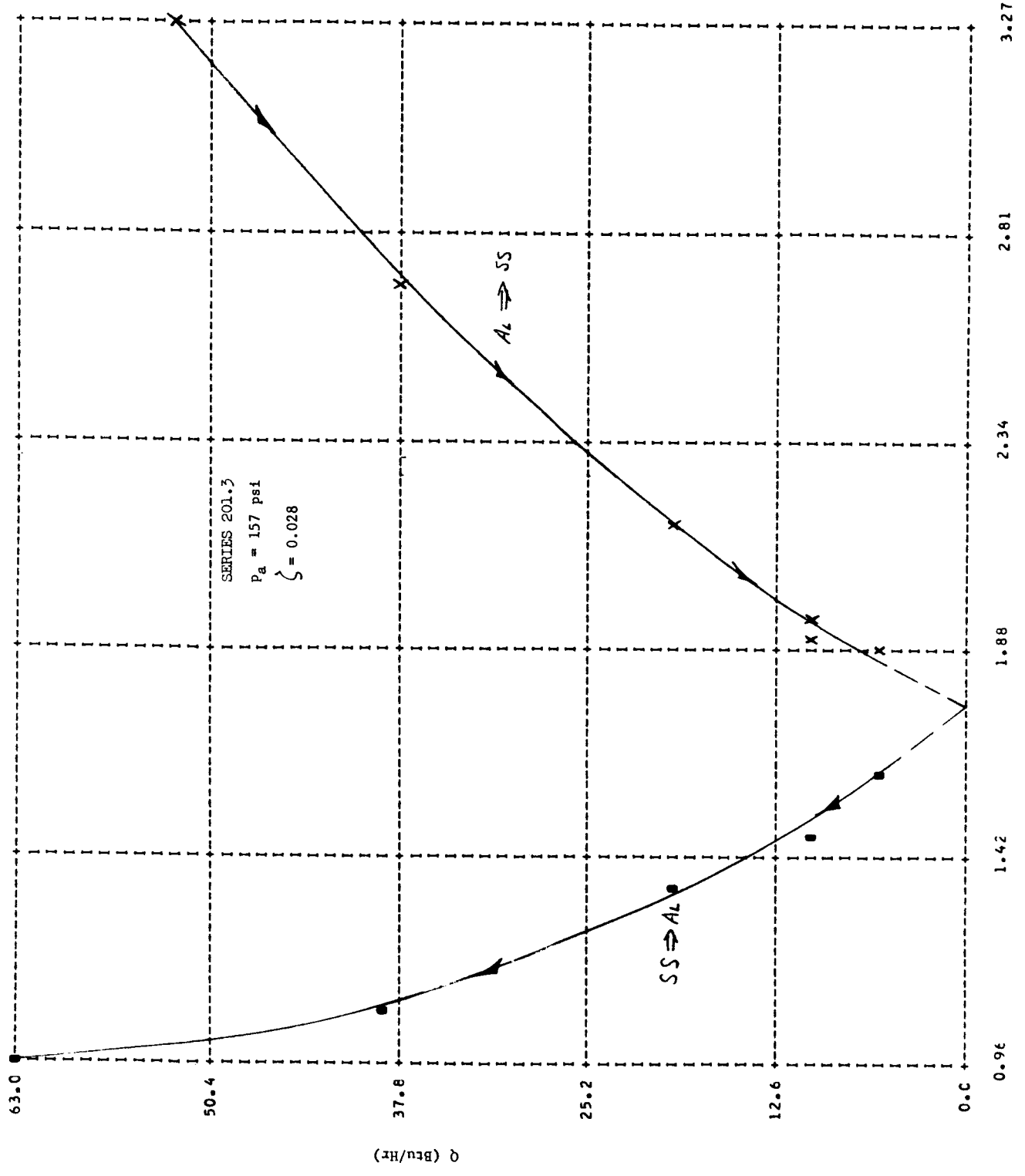

FIGURE 2.5. THE INFLUENCE OF THE RATE OF HEAT FLOW ON THE CONTACT RESISTANCE: STAINLESS STEEL-ALUMINUM INTERFACE

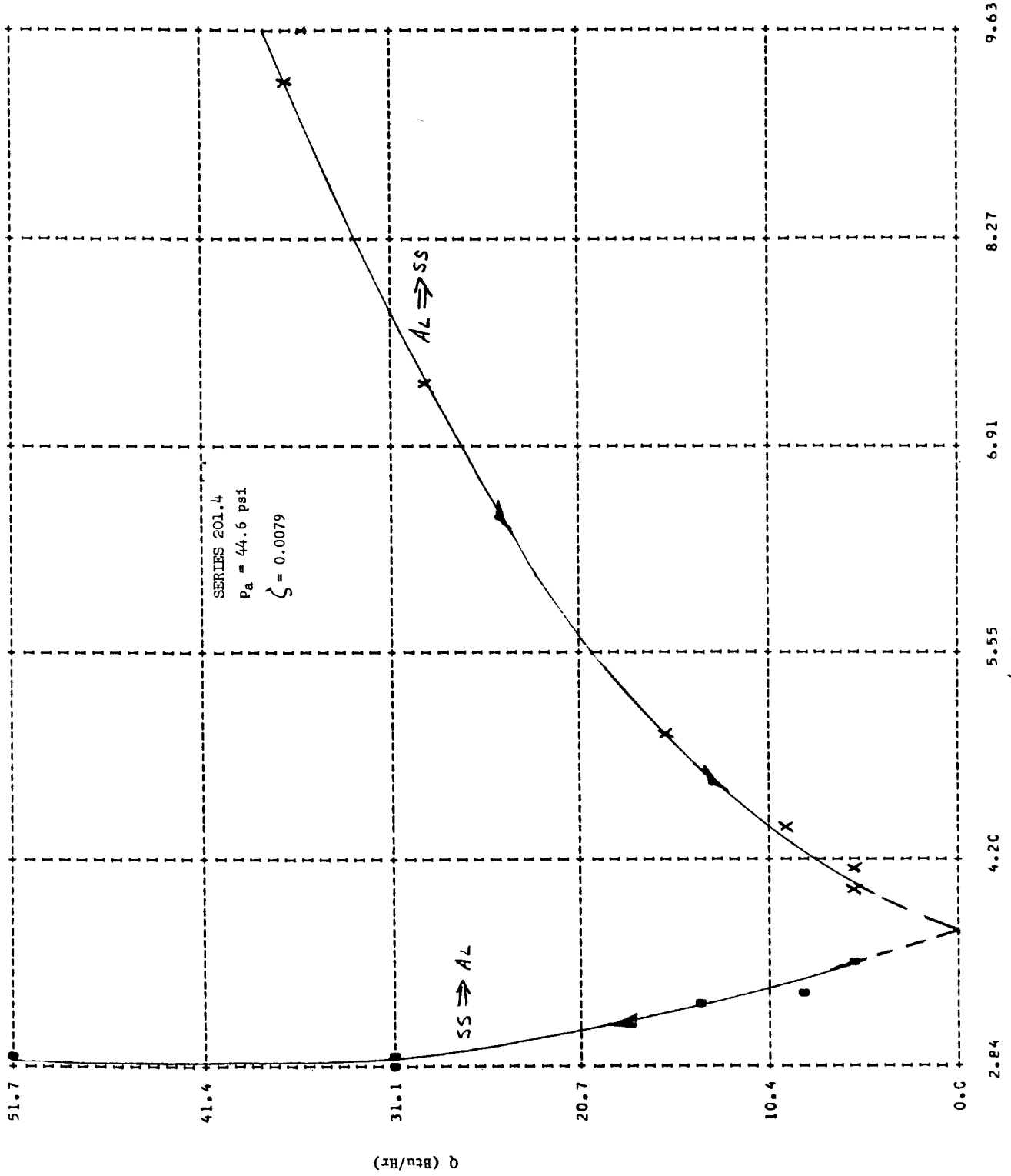

FIGURE 2.6. THE INFLUENCE OF THE RATE OF HEAT FLOW ON THE CONTACT RESISTANCE: STAINLESS STEEL-ALUMINUM INTERFACE

varied with the rate of heat flow from approximately 100°F to 400°F. Since the specimen surfaces were polished to reduce the radiation heat loss, the thermal strain due to the macroscopic constriction caused the dominant directional effect. However, it is believed that the influence of the thermal strain due to the radiation heat losses can also be seen. For example, the change in the dimensionless resistance $R^* = (\Delta L_m/b_L)$ with the rate of heat flow Q; i.e., dR^*/dQ, is either positive or negative depending on the direction of heat flow; however, d^2R^*/dQ^2 is always positive. The fact that d^2R^*/dQ^2 is always positive is probably due to the radiation heat losses. Figures 2.4 and 2.5 also show that for the case when heat flowed from stainless steel to aluminum, dR^*/dQ approached zero for large values of Q. Perhaps if Q were sufficiently large, the thermal strain due to heat losses would dominate, and dR^*/dQ would be positive.

The agreement between the theory of [1] and the dimensionless resistances of Figures 2.4, 2.5, and 2.6 is good if the heat flux is near zero. Therefore, the present theory can also be applied to dissimilar metals, provided that the effects of thermal strain are small.

Another series of tests were made, identical to those previously described except that the aluminum specimen was replaced by a magnesium specimen. These results are presented in Figures 2.7, 2.8, and 2.9. The general trends and the signs of dR^*/dQ and d^2R^*/dQ^2 are the same as those experienced before the magnesium was substituted for the aluminum. The agreement between the theoretically predicted resistances and the experimental values for low rates of heat flow was not as good as previously experienced. This was probably due to the creep which took place in the magnesium specimen; thus, the conformity of the surfaces improved and the predicted resistances were too large.

From Figures 2.4 through 2.9, it can be seen that for both interfaces at the higher rates of heat flow a variation in the contact resistance of approximately

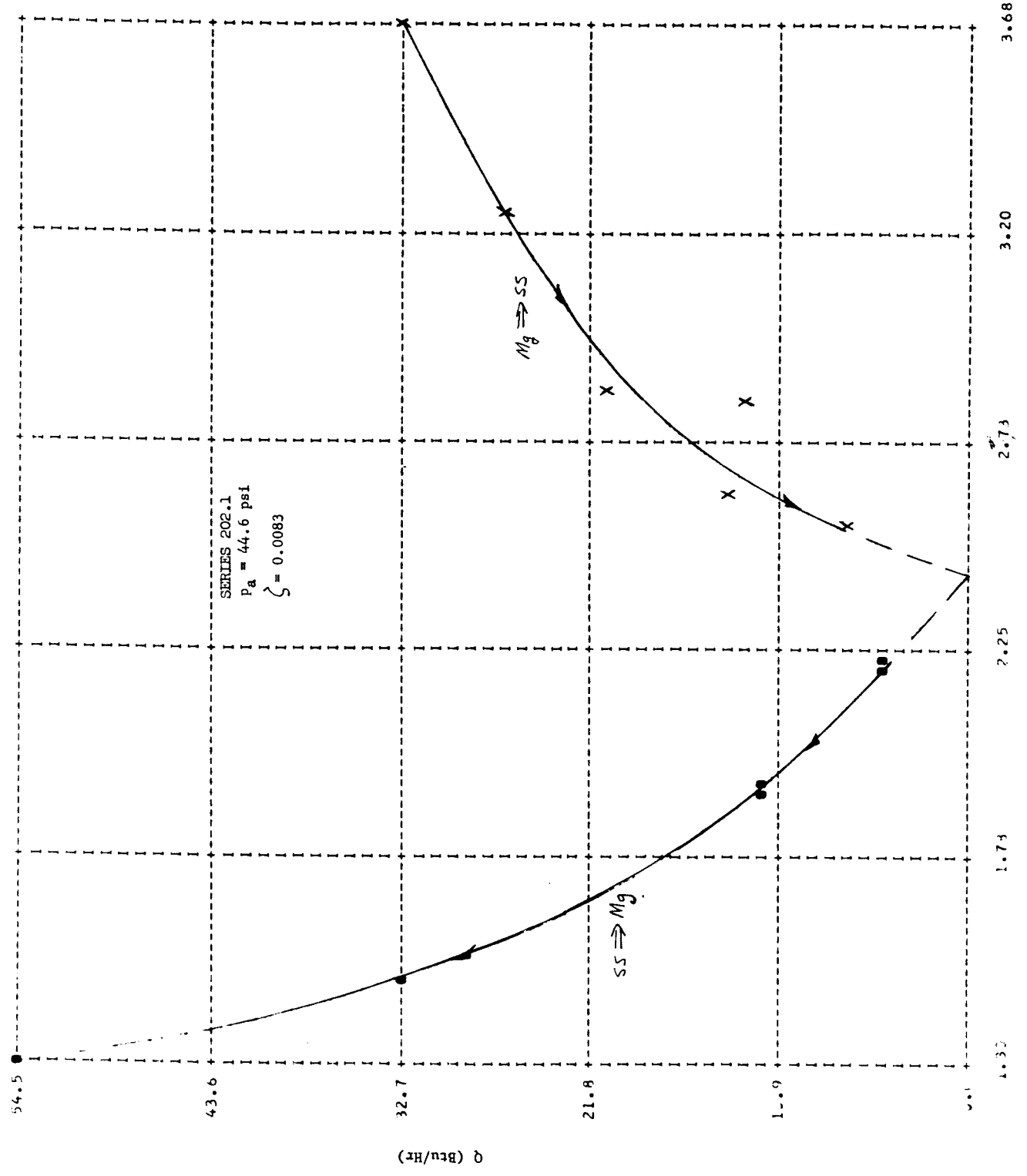

FIGURE 2.9. THE INFLUENCE OF THE RATE OF HEAT FLOW ON THE CONTACT RESISTANCE: STAINLESS STEEL-MAGNESIUM

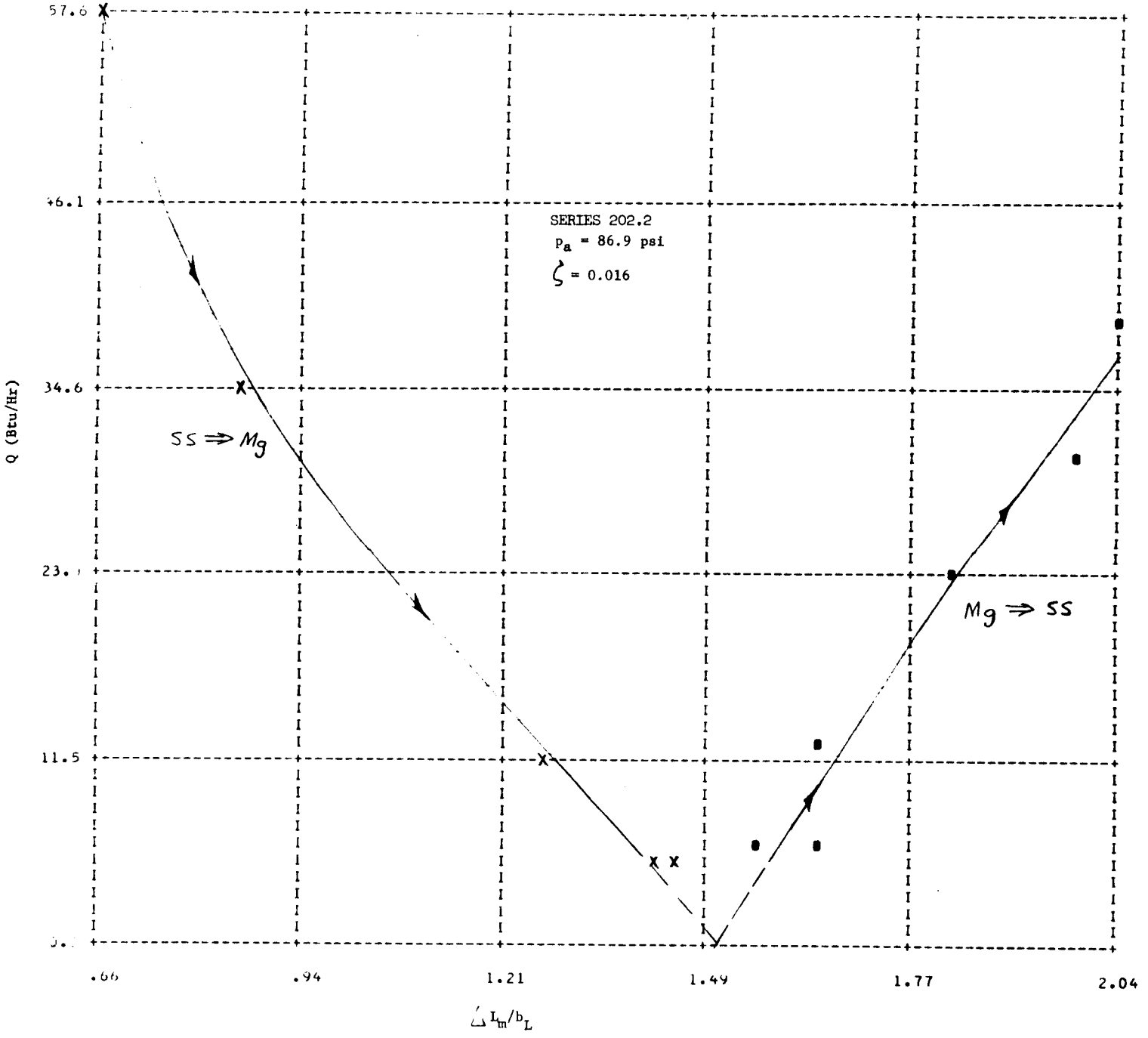

FIGURE 2.7. THE INFLUENCE OF THE RATE OF HEAT FLOW ON THE CONTACT RESISTANCE: STAINLESS STEEL-MAGNESIUM INTERFACE

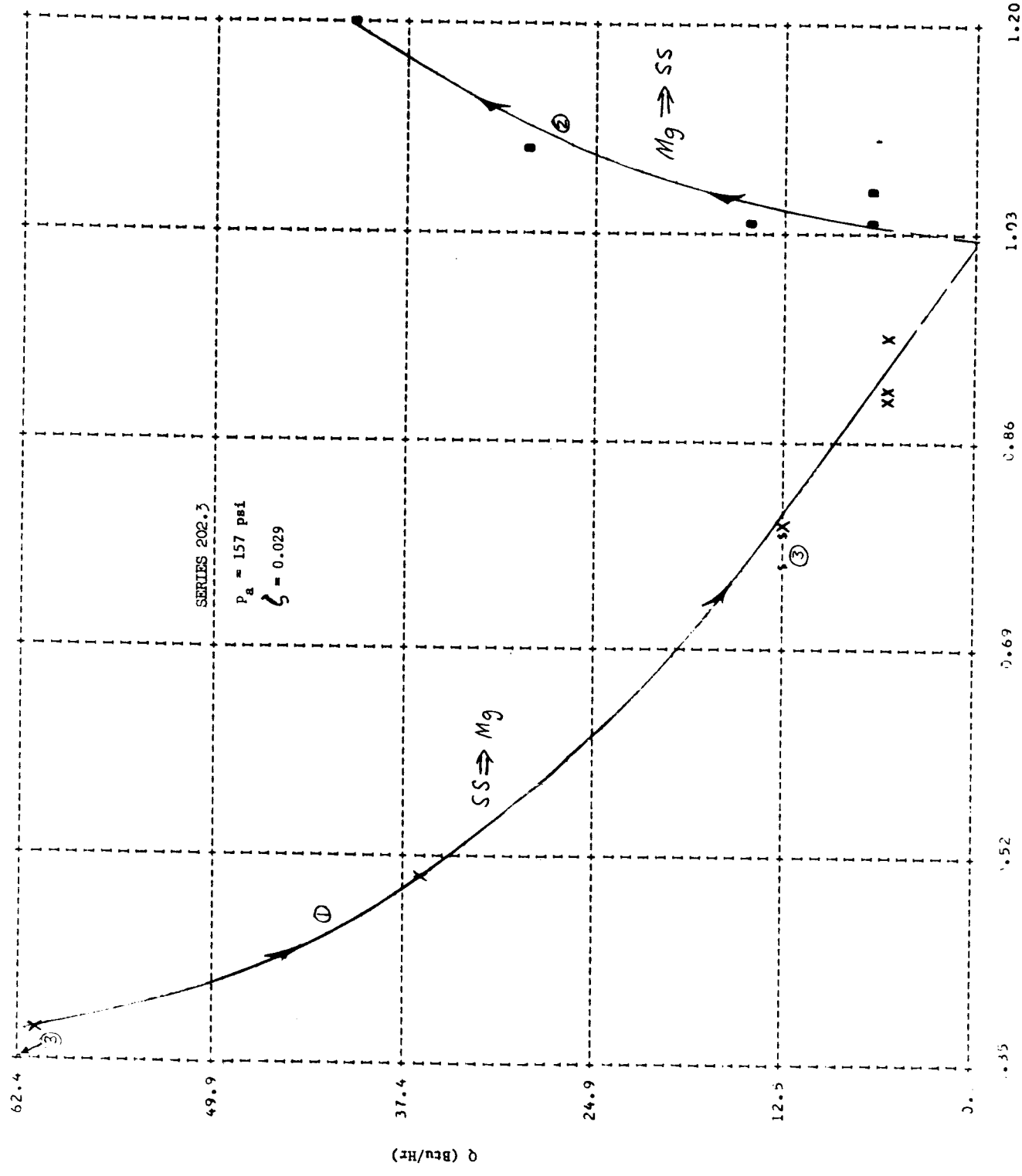

FIGURE 2.8. THE INFLUENCE OF THE RATE OF HEAT FLOW ON THE CONTACT RESISTANCE: STAINLESS STEEL-MAGNESIUM INTERFACE

300% occurred with the reversal of the direction of heat flow. On the other hand, the directional effect was negligible for low rates of heat flow.

Plots of rate of heat flow versus resistance were employed since these plots are believed to be more meaningful than the temperature versus resistance or conductance plots employed in the literature. However, it must be remembered that the mean interface temperature varied considerably in these tests. This caused large variations in the thermal conductivity, the coefficient of linear expansion, the modulus of elasticity, and other properties. The effects of property variations with temperature in many instances have been removed by employing dimensionless coordinates.

It can now be seen that some of the discrepancies between experimental data and theory reported in [1] may have been partially due to the influence of thermal strain, especially for the very flat surfaces. Previously, discrepancies were usually attributed to the neglect of microscopic effects. Microscopic effects are still believed to be of importance in some instances.

The directional trend which was found in this investigation for the stainless steel-aluminum interface is opposite to that found by Barzelay, et al. [3], and Rogers [4]. This is believed to be a consequence of the dominance of thermal strain due to the thermal environment in their experimental results in contrast to that resulting from the macroscopic constriction which dominated the present results. Their results are difficult to explain completely without more information on their test procedure and apparatus. Powell's [7] failure to detect a directional effect was probably due to a combination of the geometry and the small rate of heat flow which was employed; thus, thermal strain was not of importance.

A considerable amount of work was spent on the study of the effect of radial gradients; however, the results were inconclusive. A brief discussion of this study follows.

The specimens in the thermal contact resistance apparatus employed are unguarded (see [1] for a complete description of the apparatus). Thus, small radial gradients occur in the specimens as a consequence of radiation heat exchange with the surroundings. The radial gradients are small, since: (i) there is no insulation nor an alignment device in contact with the specimens which would otherwise provide a heat shunt; (ii) the specimens are highly polished and therefore have low emissivity surfaces; and (iii) the vacuum environment reduces the convective heat exchange to a negligible amount. These sources of radial gradients were often present in the test apparatus employed by other investigators who reported a directional effect.

A guard was constructed for the test apparatus in order to vary the radial temperature gradient. The guard consisted of a two-inch diameter copper tube which was electrically heated by nichrome wire windings. It was concentrically located around the lower specimen and guarded only the lower specimen. It was approximately isothermal; i.e., no attempt was made to match the gradient present in the specimen. Ideally, the $\partial T/\partial r$ is approximately zero away from the disturbances of the interfaces. The addition of the guard made it possible to obtain a small radial heat flow in either direction.

It was thought that the small gradients which one could obtain in this manner would be sufficient to establish clearly the importance of thermal strain resulting from the thermal environment. However, several difficulties were encountered. The basic problems were:

(i) The addition of the guard caused error in the heat loss calibration curves. Also, some heat exchange occurred between the guard and the source, which in some cases were in light physical contact.

and (ii) Curvature in the gradient due to heat exchange with the environment caused errors in the determination of the extrapolated surface temperatures and hence in the calculated contact resistance.

A new experimental apparatus, which should alleviate the above difficulties, is under construction; therefore, no attempt was made to improve the accuracy of these results. Modifications incorporated in the new facility combined with a data reduction program designed in the light of these extensions should circumvent the present problems. Further study of the influence of the thermal environment has thus been postponed until the new facility is completed.

Appendix A Tabulated Experimental Results

A.1 Units of Tabulated Quantities

p_a (psi); ΔT (^{o}F); Q (BTU/hr);

h $\left(\frac{BTU}{hr\ ft^2\ ^{o}F}\right)$; $R^* = \frac{\Delta L}{b_L}$ (dimensionless);

$\zeta = \left(\frac{p_a}{E_m}\right)\left(\frac{b_L}{d_t}\right)$ (dimensionless)

A.2 Results of Test Series 201

	Material	Surface Roughness	Flatness Deviation* (initial)	(final)
Upper Specimen:	Stainless Steel (303)	3 μ in.	14	14
Lower Specimen:	Aluminum (2024)	3 μ in.	1.5	3**

* Flatness deviation is given in fringes. One fringe is 11.6 microinches.

** After the completion of the test series with this specimen, it had a "hole" at the center portion of its surface which was approximately 6 μ inches deep.

Total Equivalent Flatness Deviation (value employed in the calculation of ζ): 180 μ inches.

Series 201.1 Object: To determine the variation of the interface conductance with contact pressure for a contact between dissimilar materials. The total temperature drop was approximately constant throughout the test series.

Test No.*	p_a	h	ΔT	Q	$\zeta \times 10^4$	R*
1	29.2	66.3	110.2	39.8	53	6.19
2	67.7	148	62.2	50	122	2.73
3	157	328	32.1	57.5	282	1.22
4	311	633	18.1	62.5	560	.63
5	519	1238	10.1	67.9	934	.32
6	760	1730	7.1	67.2	1369	.23
7	311	741	15.4	62.4	560	.54
8	67.7	160	58.8	51.4	122	2.52
- 9	29.2	29.4	185	29.6	57	14.00
- 10	67.7	57.6	129	40.6	131	7.28
- 11	157	124	77	51.9	305	3.43
- 12	311	220	48	57.4	604	1.95
- 13	519	355	31.3	60.5	1008	1.22
- 14	760	543	21.2	62.6	1478	.80
- 15	987	736	15.8	63.3	1919	.59
- 16	519	356	30.9	60.0	1008	1.21
- 17	157	128	74.7	52.1	305	3.34
- 18	29.2	30.5	181.9	30.3	57	13.49

* Sign denotes the direction of heat flow. Positive sign indicates heat is flowing from the upper specimen to the lower specimen.

Series 201.2 through 201.4 Object: To determine the influence of the rate of heat flow on the contact resistance for an aluminum-stainless steel interface.

Test No.	h	ΔT	Q	R*	
28	258	41.2	58.1	1.55	
29	252	30.5	41.9	1.57	
30	227	22.4	27.7	1.72	Series 201.2
31	194	12.9	13.7	1.99	p_a = 86.9
- 32	138	18.1	13.7	2.84	$\zeta \cong 0.016$
- 33	115	42.9	26.9	3.52	
- 34	92	72.0	36.1	4.50	
- 35	81	103.7	45.9	5.19	
- 36	81	104.2	46.1	5.20	
- 37	131	74.0	52.7	3.27	
- 38	154	44.5	37.3	2.69	
- 39	185	19.4	19.5	2.15	Series 201.3
- 40	206	9.3	10.5	1.90	p_a = 157
- 41	201	9.6	10.5	1.95	$\zeta \cong 0.028$
- 42	205	4.9	5.4	1.89	
43	238	4.1	5.3	1.61	
44	261	7.1	10.0	1.48	
45	289	12.1	19.0	1.34	
46	362	19.8	39.0	1.09	
47	416	27.8	63.0	.96	

Test No.	h	ΔT	Q	R*	
- 59	44.8	149	36.5	9.29	
- 60	55.7	96	29.1	7.33	
- 61	79.8	37.4	16.3	4.98	
- 62	88.3	19.3	9.3	4.43	Series 201.4
- 63	96.4	10.3	5.4	4.01	$p_a = 44.6$
- 64	93.9	10.6	5.4	4.12	$\zeta \cong .0079$
65	109.7	8.7	5.2	3.50	
66	108.4	8.8	5.2	3.54	
67	116.9	12.8	8.1	3.30	
68	120.7	22.0	14.5	3.22	
69	119.3	22.3	14.5	3.25	
70	135.9	42.0	31.1	2.90	
71	139.0	41.4	31.4	2.84	
72	137.7	69.0	51.7	2.93	

A.3 Results of Test Series 202

	Material	Surface Roughness	Flatness Deviation* (initial)	(final)
Upper Specimen:	Stainless Steel (303)	3 μin.	14	14
Lower Specimen:	Magnesium (AZ31B)	4 μin.	7.5	(see note **)

* Flatness deviation is given in fringes. One fringe is 11.6 microinches.

** The surface contour of the magnesium specimen was considerably altered from creep during the test series. The creep increased the surface conformity and consequently decreased the contact resistance.

Total Equivalent Flatness Deviation: 250 μin.
(This value is the initial value. The values of ζ given are based on this flatness deviation.)

Series 202.1 through 202.3 Object: To determine the influence of the rate of heat flow on the contact resistance for a magnesium-stainless steel interface.

Test No.	h	ΔT	Q	R*	
- 18	104	58.6	33.1	3.68	
- 19	115	43.3	27.2	3.26	
- 20	130	29.8	21.1	2.84	Series 202.1
- 21	139	17.7	13.4	2.61	p_a = 44.6
- 22	129	19.0	13.4	2.82	$\zeta \cong .0083$
- 23	141	9.0	7.0	2.53	
24	161	5.2	4.6	2.19	
25	158	5.3	4.6	2.23	
26	186	11.6	11.8	1.91	
27	183	11.8	11.8	1.94	
28	245	24.5	32.7	1.48	
29	285	35.1	54.5	1.30	
31	558	19.0	57.6	.66	
32	424	14.8	34.1	.85	
33	281	7.6	11.6	1.26	
34	247	4.1	5.6	1.43	Series 202.2
35	243	4.3	5.7	1.45	p_a = 86.9
- 36	228	5.3	6.5	1.56	$\zeta \cong 0.016$
- 37	217	5.6	6.6	1.65	
- 38	220	10.8	12.9	1.65	
- 39	204	20.3	22.5	1.82	
- 40	190	29.1	30.0	1.98	
- 41	188	37.5	38.4	2.04	

Test No.	h	ΔT	Q	R*	
42	984	11.5	61.5	.37	
43	718	9.1	35.8	.50	
44	447	5.0	12.1	.79	
45	454	4.9	12.1	.78	Series 202.3
46	394	2.8	5.9	.90	p_a = 157
47	391	2.8	5.9	.90	$\zeta \cong 0.029$
48	375	2.9	5.9	.94	
- 49	344	3.7	6.9	1.04	
- 50	336	3.8	6.9	1.06	
- 51	353	7.9	15.2	1.03	
- 52	343	16.0	29.8	1.10	
- 53	322	23.2	40.7	1.20	
- 54	331	9.0	16.1	1.10	
55	471	4.7	12.2	.75	
56	454	4.9	12.2	.78	
57	1045	11.0	62.4	.35	

Appendix B References

1. A. M. Clausing and B. T. Chao, "Thermal Contact Resistance in a Vacuum Environment," University of Illinois Engineering Experiment Station Report, ME-TN-242-1 (or, Ph.D. Dissertation by A. M. Clausing) August, 1963.

2. McCracken and Dorn, Numerical Methods and Fortran Programming, John Wiley and Sons, New York, 1964; p. 260.

3. M. E. Barzelay, K. N. Tong and G. F. Holloway, "Effect of Pressure on Thermal Conductance of Contact Joints," NACA TN-3295, May, 1955.

4. G.F.C. Rogers, "Heat Transfer at the Interface of Dissimilar Metals," Int. J. Heat Mass Transfer, Vol. 2, 1961; pp. 150-154.

5. A. Williams, "Comment on Rogers' Paper ' Heat Transfer at the Interface of Dissimilar Metals,'" Int. J. Heat Mass Transfer, Vol. 3, 1961; p. 159.

6. J. S. Moon and R. N. Keeler, "A Theoretical Consideration of Asymmetric Heat Flow at the Interface of Two Dissimilar Metals," University of California, Lawrence Radiation Laboratory Report No. 9885, October, 1961.

7. R. W. Powell, R. P. Tye and B. W. Jolliffe, "Heat Transfer at the Interface of Dissimilar Materials: Evidence of Thermal-Comparator Experiments," Int. J. Heat Mass Transfer, Vol. 5, 1962; pp. 897-902.

8. L. C. Roess, "Theory of Spreading Conductance," Appendix A of an unpublished report of the Beacon Laboratories of Texas Company, Beacon, New York.